Photochemistry of Polyoxovanadates. Part 1. Formation of the Anion-encapsulated Polyoxovanadate $[V_{15}O_{36}(CO_3)]^{7-}$ and Electron-spin Polarization of α-Hydroxyalkyl Radicals in the Presence of Alcohols†

Toshihiro Yamase* and Kawori Ohtaka
Research Laboratory of Resources Utilization, Tokyo Institute of Technology, 4259 Nagatsuta, Midori-ku, Yokohama 227, Japan

Prolonged photolysis of aqueous solutions containing $[V_4O_{12}]^{4-}$ and MeOH at pH 9 (pH adjusted by use of K_2CO_3) led to the formation of $K_5H_2[V_{15}O_{36}(CO_3)]\cdot 14.5H_2O$. A single-crystal X-ray structural analysis of dark green crystals of $K_5H_2[V_{15}O_{36}(CO_3)]\cdot 14.5H_2O$ [triclinic, space group $P\bar{1}$, $a = 12.361(4)$, $b = 18.149(5)$, $c = 11.415(4)$ Å, $\alpha = 93.44(3)$, $\beta = 107.76(3)$, $\gamma = 93.54(3)°$, $Z = 2$, $R = 0.081$ for 4182 independent data with $I > 5\sigma(I)$] showed that the pentadecavanadate encapsulates CO_3^{2-} with approximate D_{3h} symmetry and formally contains eight V^{IV} and seven V^{V} centres. The co-ordination geometries at the vanadium centres in the anion consist of twelve (V^{IV}, V^{V}) VO_5 square pyramids and three $V^{IV}O_6$ octahedra. Each of the VO_6 octahedra co-ordinates the CO_3^{2-} oxygen atoms with V–O bond lengths 2.2616(8)–2.3710(7) Å. The photochemical encapsulation of other anions such as Cl^-, Br^-, NO_3^- or PO_3^{3-} in the $[V_{15}O_{36}]^{5-}$ spherical cluster shell is observed in a similar way, which is applicable to the photofixation of CO_2. The photoinduced electron transfer to the O ⟶ V ligand-to-metal charge-transfer (l.m.c.t.) excited state of $[V_4O_{12}]^{4-}$ from alcohols such as MeOH, EtOH or PrⁱOH was investigated with chemically induced dynamic electron polarization (CIDEP) with 100 ns time resolution. The formation and decay of α-hydroxyalkyl radicals, following pulsed-laser excitation of the polyoxometalate was also observed for $[Mo_7O_{24}]^{6-}$ and $[W_{10}O_{32}]^{4-}$. Observation of an emissive CIDEP ESR pattern for the α-hydroxyalkyl radicals revealed that the reaction precursor is the excited triplet state of the O ⟶ M (M = V, Mo or W) l.m.c.t. which undergoes hydrogen abstraction from alcohols to yield the one-protonated reduced polyoxometalate (for example $[V_4O_{12}H]^{4-}$) and the α-hydroxyalkyl radical. The absence of distortion in the ESR polarization of α-hydroxyalkyl radicals and the external magnetic field effect indicated that the interaction between $[V_4O_{12}H]^{4-}$ and α-hydroxyalkyl radicals is extremely weak in water.

Ultraviolet irradiation of aqueous solutions containing polyoxovanadate and alcohols at pH 9 leads to H_2 formation (quantum yield 2×10^{-3}) with an accompanying formation of two-electron alcohol-oxidation species.[1] Under the experimental conditions required for the optimum yield of H_2 [4.6 mmol dm^{-3} total V^{V} in H_2O–MeOH = 5:1 (v/v) at pH 9] the predominant and photoresponsive vanadate ion has been proposed to be the divanadate ion in equilibrium with the tetravanadate ion.[2,3] Observable luminescence from the oxygen-to-metal (O ⟶ M) ligand-to-metal charge-transfer (l.m.c.t.) triplet states of polyoxometalates of tungsten and molybdenum below 100 K in the solid state let us propose the involvement of the O ⟶ M l.m.c.t. triplet state in the photoredox reaction in solution.[4] In this case, the low quantum yield of H_2 for the polyoxovanadate system may arise from the small yield of the excited triplet state of the O ⟶ V l.m.c.t. state due to the small spin-orbit coupling of vanadium compared to tungsten and molybdenum. However, luminescence from the O ⟶ M l.m.c.t. excited triplet states in solution was not observed, probably due to the hydrogen-bonding quenching of the excited states, making their involvement in the solution photochemistry of polyoxometalates uncertain.[4] Two cyclic tetravanadates, $[NBu_4]_3[HV_4O_{12}]$ and $[NH_3Bu^t]_4[V_4O_{12}]$ have been crystallographically characterized.[5,6] The $[V_4O_{12}]^{4-}$ anion is the main species existing in the region of pH 8–10 at high concentrations (> 10 mmol dm^{-3}) of vanadates[3] and we have found that prolonged photolysis of aqueous solutions containing $[V_4O_{12}]^{4-}$ and MeOH at pH 9 (pH adjusted by use of K_2CO_3) gave an inclusion complex $K_5H_2[V_{15}O_{36}(CO_3)]\cdot 14.5H_2O$ with an accompanying formation of formaldehyde and H_2. The same anion has been reported for $Li_7[V_{15}O_{36}(CO_3)]\cdot ca.39H_2O$ produced by the thermal reaction of V_2O_5, Li_2CO_3 and $(H_2NNH_3)_2SO_4$.[7] However, unlike the photolysis product, the CO_3^{2-} group in this anion was disordered over two positions.

This paper describes the X-ray crystallographic characterization of the eight-electron reduced polyoxovanadate $K_5H_2[V_{15}O_{36}(CO_3)]\cdot 14.5H_2O$, which is photochemically produced from the $[V_4O_{12}]^{4-}$–MeOH system at pH 9. In addition, the chemically induced dynamic electron polarization (CIDEP) phenomena for the $[V_4O_{12}]^{4-}$–, $[Mo_7O_{24}]^{6-}$– and $[W_{10}O_{32}]^{4-}$–alcohol systems are described, which allows us to detect large electron-spin polarization of α-hydroxyalkyl radicals generated by the transfer of electron polarization from the precursor, and to investigate the primary photoredox processes of polyoxometalates in solution. There are two main mechanisms of generating CIDEP in free radicals,[8–10] one being the triplet and the other the radical-pair mechanism. Most CIDEP spectra are interpreted by a combination of these two mechanisms. If the photoredox reaction of polyoxometalates involves the O ⟶ M l.m.c.t. triplet state, triplet-spin polarization can be carried over to free radical products and give rise to CIDEP. To

† *Supplementary data available:* see Instructions for Authors, *J. Chem. Soc., Dalton Trans.*, 1994, Issue 1, pp. xxiii–xxviii.

be observed, radical production must take place before thermal equilibrium of the triplet spin-lattice relaxation has been established. Spin polarization can also be generated by the time evolution of the spin state of precursor radical pairs. The time evolution of signal amplitudes in this radical-pair mechanism will not only reflect variations in radical concentrations but also the properties of precursor radical pairs and the spin-lattice relaxation time in doublet radical products.

Experimental

Materials, Preparations and Spectral Measurements.—All the reagents were of at least analytical grade and were used without further purification. The polyoxometalates $[NH_3Bu^t]_4[V_4O_{12}]$ and $[NBu_4]_4[W_{10}O_{32}]$ were synthesized according to published procedures and identified in the solid state by comparison of their IR spectra with those previously reported.[6,11] Preparation of $K_5H_2[V_{15}O_{36}(CO_3)]\cdot 14.5H_2O$ **1** was as follows. The polyoxometalate $[NH_3Bu^t]_4[V_4O_{12}]$ (1.6 g, 2.3 mmol) was dissolved in water (40 cm^3) in a Pyrex tube (50 cm^3) to give pH 6.8. To adjust the pH to 9.4 K_2CO_3 was added and then MeOH (4 cm^3). The resulting solution was irradiated for 2 d under an atmosphere of nitrogen using a 500 W superhigh-pressure mercury lamp and an aqueous solution of saturated KCl (4 cm^3) was added to the dark green photolyte to yield **1** (0.5 g). Dark green single crystals of the photoreduced product were precipitated within 1 d after photolysis. The vanadium content of **1** was determined using the potentiometric method by detecting the end-points of titrations with Ce^{4+} (for V^{IV}) and Fe^{2+} (for V^V) in stirred H_2SO_4 (2 mol dm^{-3}) solutions: measurements of the potential using a Pt indicator electrode *vs.* an Ag–AgCl reference electrode in an open circuit were carried out using a TOA Electronics IM-5S ion meter.[12] Analysis of V^{IV} in **1** could be also determined by titration with $KMnO_4$ under an atmosphere of nitrogen [indicating a composition corresponding to nearly eight electron reduction (*ca.* eight V^{IV} per fifteen V atoms]. Potassium was determined potentiometrically by a use of a TOA Electronics IM-5S ion meter and thermogravimetric analysis (Rigaku, Thermoflex TG-DGC) determined the water of crystallization (Found: C, 0.70; K, 10.80; V, 36.35. Calc. for $CH_{31}K_5O_{53.5}V_{15}$: C, 0.65; K, 10.50; V, 41.10%). Complex **1** could also be obtained by a modification of the above procedure. The vanadate Na_3VO_4 (1 g, 5.4 mmol) was dissolved in water (20 cm^3) to give pH 11.5. Carbon dioxide gas was flushed into the alkaline solution to adjust the pH to 8.3 and then MeOH (2 cm^3) was added. The same procedures for the photolysis and crystallization result in the formation of complex **1**. Other anion-encapsulated pentadecavanadates containing Cl^-, Br^-, NO_3^- or PO_3^{3-} were similarly synthesized by this modified procedure.

CIDEP measurements were performed at room temperature by a JEOL X-band ESR spectrometer without field modulation. A CIDEP sample in a microwave cavity was irradiated with a Questek 2320 excimer XeCl (308 nm, 50 mJ per pulse, with a repetition rate of 30 Hz) laser. The photoinduced transient ESR signals amplifed by a preamplifier of a microwave unit (JEOL RE-IX) were fed to a NF BX-531 boxcar integrator, and spectra were measured 0.2–1.6 μs after the laser pulse. Sample solutions were bubbled with nitrogen gas to remove dissolved oxygen in solutions and flowed through a quartz flat cell (0.3 mm interior space) at a flow rate of *ca.* 25 cm^3 min^{-1}. The time resolution of our CIDEP set up was *ca.* 0.1 μs.

X-Ray Structural Analysis of $K_5H_2[V_{15}O_{36}(CO_3)]\cdot 14.5H_2O$ **1**.—*Crystal data.* $CH_{31}K_5O_{53.5}V_{15}$, $M = 1858.8$, triclinic, space group $P\bar{1}$, $a = 12.361(4)$, $b = 18.149(5)$, $c = 11.415(4)$ Å, $\alpha = 93.44(3)$, $\beta = 107.76(3)$, $\gamma = 93.54(3)°$, $U = 2426(3)$ $Å^3$, $Z = 2$, $D_c = 2.554$ g cm^{-3} $F(000) = 1806$ and μ(Mo-Kα) = 32.11 cm^{-1}. A crystal with approximate dimensions 0.2 × 0.2 × 0.1 mm was mounted on a Rigaku AFC-5 diffractometer. The orientation matrix and cell dimensions were obtained from the setting angles of 20 centred reflections in the 2θ range 17.5–29.6°. Intensities were collected in the range $2 \leqslant 2\theta \leqslant 60°$ using graphite-monochromatized Mo-Kα ($\lambda = 0.710\,69$ Å) radiation and the ω–2θ scan technique at the 2θ scan rate of 8° min^{-1}. No significant decay of intensity of the three standard reflections recorded after every 100 reflections was observed. Of 14 174 independent reflections, 4182 having $I > 5\sigma(I)$ were retained for the refinement of the structure. The vanadium positions were determined by a direct method using MITHRIL,[13] and the potassium oxygen, and carbon atoms were located from difference syntheses. Lorentz and polarization factors were applied and an absorption correction was made based on the isotropically refined structure, using the program DIFABS.[14] The correction factors were 0.64–1.25. Subsequently the vanadium and potassium atoms were refined with anisotropic thermal parameters. Refinements were carried out using the full-matrix least-squares method for 421 parameters. The quantity minimized was $\Sigma w(|F_o| - |F_c|)^2$. Attempts were made to refine the crystal water oxygen atoms with various combinations of site-occupancy factors. The refinement converged at $R = R' = 0.081$ $\{R = \Sigma(|F_o| - |F_c|)/\Sigma|F_o|$, $R' = [\Sigma w(|F_o| - |F_c|)^2/\Sigma w|F_o|^2]^{\frac{1}{2}}\}$; the weighting scheme employed was $w^{-1} = \sigma^2(F_o)$, where $\sigma^2(I_0) = \sigma^2(I_{counting}) + (0.03\ I_0)^2$, $S = \Sigma w^{\frac{1}{2}}(|F_o| - |F_c|)^2/(n - m) = 4.38$, and $(\Delta/\sigma)_{max} = 0.377$. The maximum and minimum heights in the final difference synthesis were 2.3 and −0.9 e $Å^{-3}$, respectively. All calculations were carried out on a Micro VAX II computer using the TEXSAN software package.[15]

Additional material available from the Cambridge Crystallographic Data Centre comprises thermal parameters and remaining bond lengths and angles.

Results

IR Spectrum of Complex **1**. The IR spectrum (KBr disc) of $K_5H_2[V_{15}O_{36}(CO_3)]\cdot 14.5H_2O$ **1** is shown in Fig. 1 Bands are at 1630m, 1460m, 953s, 845w, 739m and 623s cm^{-1}. The photolysis of aqueous solutions containing Na_3VO_4 (1 g) and MeOH (2 cm^3) at pH 9 (due to CO_2 flushing) results in the formation of complex **1**, identified by its IR spectrum. This indicates the occurrence of photofixation of CO_2 by the polyoxovanadate system. Furthermore, similar IR spectra were obtained for the Cl^--, Br^--, NO_3^-- or PO_3^{3-}-encapsulated pentadecavanadate solids prepared by the addition of HCl,

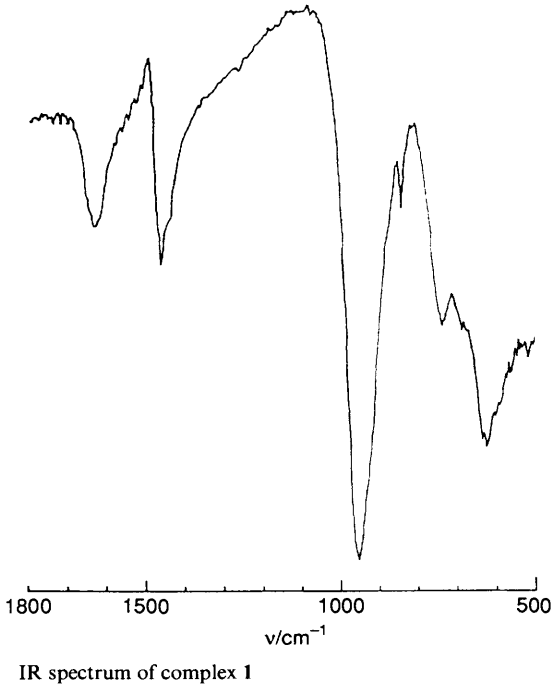

Fig. 1 IR spectrum of complex **1**

Table 1 Atomic coordinates for complex **1** with estimated standard deviations (e.s.d.s) in parentheses

Atom	x	y	z	Atom	x	y	z
V(1)	0.3029(4)	0.3312(2)	0.5293(4)	O(21)	0.032(1)	0.4011(7)	0.238(1)
V(2)	0.0557(4)	0.3532(2)	0.3922(4)	O(22)	0.030(1)	0.1430(8)	0.312(1)
V(3)	0.0933(4)	0.0883(2)	0.1952(4)	O(23)	−0.006(1)	0.1481(8)	0.087(1)
V(4)	−0.0646(4)	0.2051(2)	0.2019(4)	O(24)	0.202(1)	0.0937(8)	0.110(1)
V(5)	0.4473(4)	0.2587(2)	0.1357(4)	O(25)	0.229(1)	0.1043(8)	0.336(1)
V(6)	0.2605(4)	0.1444(2)	−0.0025(4)	O(26)	−0.067(1)	0.2733(7)	0.076(1)
V(7)	0.4640(4)	0.3866(2)	0.3239(4)	O(27)	0.522(1)	0.2861(8)	0.319(1)
V(8)	0.1829(4)	0.4544(2)	0.2911(4)	O(28)	0.431(1)	0.3649(8)	0.145(1)
V(9)	0.3077(4)	0.4299(2)	0.1026(4)	O(29)	0.403(1)	0.1498(7)	0.131(1)
V(10)	0.4677(4)	0.2452(2)	0.4461(4)	O(30)	0.317(1)	0.2409(8)	−0.024(1)
V(11)	0.0114(4)	0.3684(2)	0.0658(4)	O(31)	0.123(1)	0.1897(7)	−0.064(1)
V(12)	−0.0202(4)	0.2141(2)	−0.0423(4)	O(32)	0.331(1)	0.4409(7)	0.280(1)
V(13)	0.3421(4)	0.1012(2)	0.2485(4)	O(33)	0.144(1)	0.4536(7)	0.102(1)
V(14)	0.1837(4)	0.1760(2)	0.4416(4)	O(34)	0.246(1)	0.3788(8)	−0.057(1)
V(15)	0.1780(4)	0.2867(2)	−0.0995(4)	O(35)	0.457(1)	0.1504(8)	0.383(1)
K(1)	0.2045(6)	0.5182(3)	0.5988(6)	O(36)	0.034(1)	0.3113(7)	−0.081(1)
K(2)	0.5857(6)	0.4149(3)	0.6519(7)	O(37)	0.303(1)	0.2424(8)	0.232(1)
K(3)	0.1970(6)	−0.0525(4)	0.0238(7)	O(38)	0.183(1)	0.3221(8)	0.140(1)
K(4)	0.0340(6)	0.1077(3)	0.7054(6)	O(39)	0.155(1)	0.2588(8)	0.293(1)
K(5)	0.0713(8)	0.6610(4)	0.3270(7)	O(40)	0.323(2)	0.861(1)	0.661(2)
O(1)	0.358(1)	0.3664(8)	0.669(1)	O(41)	0.374(2)	0.838(2)	0.126(3)
O(2)	−0.004(1)	0.4011(8)	0.477(1)	O(42)	0.102(2)	0.468(1)	0.767(2)
O(3)	0.041(1)	0.0032(9)	0.170(2)	O(43)	0.472(1)	0.3649(7)	0.908(1)
O(4)	−0.188(1)	0.1660(9)	0.167(2)	O(44)	0.404(2)	0.199(1)	0.764(2)
O(5)	0.557(2)	0.254(1)	0.087(2)	O(45)	0.097(2)	0.799(1)	0.470(2)
O(6)	0.266(1)	0.0850(9)	−0.110(2)	O(46)	0.086(2)	−0.033(1)	−0.399(2)
O(7)	0.571(1)	0.4470(9)	0.383(2)	O(47)	0.246(2)	0.673(1)	0.609(2)
O(8)	0.183(1)	0.5385(9)	0.340(2)	O(48)	0.444(2)	−0.067(1)	−0.062(2)
O(9)	0.363(1)	0.506(1)	0.078(2)	O(49)	−0.432(7)	0.927(5)	0.356(8)
O(10)	0.575(1)	0.2492(9)	0.570(2)	O(50)	0.633(3)	−0.021(2)	0.272(3)
O(11)	−0.089(1)	0.4169(8)	−0.008(1)	O(51)	0.476(4)	0.056(2)	0.559(4)
O(12)	−0.125(1)	0.1791(8)	−0.162(2)	O(52)	0.213(2)	0.969(1)	0.449(3)
O(13)	0.379(2)	0.017(1)	0.251(2)	O(53)	0.331(3)	0.013(2)	0.703(3)
O(14)	0.173(1)	0.1325(8)	0.555(1)	O(54)	0.669(2)	0.121(1)	0.647(2)
O(15)	0.153(1)	0.2737(9)	−0.246(2)	O(55)	0.277(3)	0.667(2)	0.951(3)
O(16)	0.338(1)	0.2285(7)	0.510(1)	O(56)	0.355(3)	0.555(2)	0.841(3)
O(17)	0.211(1)	0.4005(7)	0.436(1)	O(57)	0.694(3)	0.325(2)	0.843(3)
O(18)	0.419(1)	0.3472(8)	0.453(1)	O(58)	0.754(2)	0.352(1)	1.130(2)
O(19)	0.141(1)	0.2792(7)	0.516(1)	O(59)	0.382(3)	0.490(2)	0.844(3)
O(20)	−0.062(1)	0.2741(8)	0.316(1)	C(1)	0.212(2)	0.274(1)	0.223(2)

HBr, HNO_3 or H_3PO_3 to the Na_3VO_4 solution, respectively, with the NO_3^--encapsulated complex showing an additional strong band at 1386 cm^{-1}. Thus, the strong broad band at *ca.* 950 cm^{-1} is due to V–O stretching for the spherical cluster shell formed by linking VO_5 pyramids (as shown below) and the intense feature at 845–623 cm^{-1} is attributed to symmetric and asymmetric stretching of V–O–V bonds.

Single-crystal Structural Analysis of the CO_3^{2-}*-Encapsulated Species.*—The unit cell contains two $K_5H_2[V_{15}O_{36}(CO_3)]\cdot 14.5H_2O$ molecules which are related by a crystallographic inversion centre. The $[V_{15}O_{36}(CO_3)]^{7-}$ anion is a nearly spherical $V_{15}O_{36}$ cluster shell encapsulating negatively charged CO_3^{2-} and formally contains eight V^{IV} and seven V^V centres. Atomic coordinates, selected bond distances and angles, and selected interatomic separations (≤2.8 Å) for complex **1** are shown in Tables 1–3, respectively. Figs. 2 and 3 show the structure of the $[V_{15}O_{36}(CO)_3)]^{7-}$ anion with atom labelling and its stereoscopic projection, respectively. The anion has approximately D_{3h} symmetry which shows a three-fold symmetry axis perpendicular to the mirror plane nearly including CO_3^{2-}. The three oxygen atoms, O(37), O(38) and O(39), of the central CO_3^{2-} group each form weak covalent bonds with the V(5), V(11) and V(14) atoms at distances of 2.3710(7), 2.2616(8) and 2.2933(7) Å, respectively, with a resultant octahedral co-ordination of oxygen atoms at these vanadium centres. Other vanadium atoms exhibit a tetragonal-pyramidal co-ordination to the oxygen atoms. The same anion has been reported for $Li_7[V_{15}O_{36}(CO_3)]\cdot ca.39H_2O$ prepared by the thermal reaction of V_2O_5, Li_2CO_3 and $(H_2NNH_3)_2SO_4$ at 80 °C.[7] However, the description of the CO_3^{2-} encapsulation in the $[V_{15}O_{36}(CO_3)]^{7-}$ anion is different from that of $Li_7[V_{15}O_{36}(CO_3)]\cdot ca.39H_2O$, as the central CO_3^{2-} group in the lithium complex was disordered over two positions related by a 60° rotation within a fixed vanadate framework. The structural difference between the two anions indicates that anions of this type offer many opportunities for isomerism.

X-Ray structural analysis of complex **1** reveals the presence of five K^+ cations per $[V_{15}O_{36}(CO_3)]^{7-}$ anion. In conjunction with the fact that the anion contains eight V^{IV} centres, this indicates the composition $K_5H_2[V_{15}O_{36}(CO_3)]\cdot 14.5H_2O$, to maintain electrical neutrality. The relative strengths of the V–O interactions are given in Table 4, where the bond strength (s) in valence units is calculated using $s = (d/1.791)^{-5.1}$ or $(d/1.770)^{-5.2}$ for the V^V–O or V^{IV}–O bond length (d) in Å, respectively, and the valence sum (bond order = Σs) of all V–O bond strengths about a given V or O atom gives the valence of the atom.[16] The alternative expression, $s = \exp[(d_0 - d)/B]$, where d_0 (= 1.803 and 1.784 Å for V^V and V^{IV} site, respectively) and B (= 0.37) are empirically determined parameters, gave similar bond-valence values.[17] Valence-sum calculations are consistent with +4 for the V(1), V(2), V(3), V(5), V(8), V(11), V(12) and V(14) centres. The valence sums of the V–O bond strengths for O(19) and O(33) are 1.1(1) and 1.3(1), respectively. By contrast, the valence sums for other oxygen atoms that carry formal negative charge in the anion are 1.6(1)–2.0(1). Smaller

Table 2 Selected bond lengths (Å) and angles (°) for complex **1** with e.s.d.s in parentheses

V(1)–O(1)	1.6084(7)	V(5)–O(28)	1.9498(5)	V(9)–O(34)	1.9069(8)	V(13)–O(35)	1.8742(8)
V(1)–O(17)	1.9000(7)	V(5)–O(29)	2.0106(5)	V(9)–O(28)	1.9498(7)	V(13)–O(25)	1.9439(6)
V(1)–O(18)	1.9051(6)	V(5)–O(30)	2.0271(9)	V(9)–O(32)	1.9501(7)	V(13)–O(24)	1.9464(8)
V(1)–O(16)	1.9527(5)	V(5)–O(27)	2.0320(8)	V(9)–O(33)	2.0954(7)	V(13)–O(29)	1.9557(6)
V(1)–O(19)	2.1204(8)	V(5)–O(37)	2.3710(7)	V(10)–O(10)	1.6122(7)	V(14)–O(14)	1.5912(5)
V(2)–O(2)	1.6235(5)	V(6)–O(6)	1.6046(5)	V(10)–O(35)	1.8079(5)	V(14)–O(25)	1.9473(6)
V(2)–O(20)	1.9362(8)	V(6)–O(31)	1.8898(7)	V(10)–O(27)	1.9354(6)	V(14)–O(16)	1.9789(8)
V(2)–O(17)	1.9568(7)	V(6)–O(30)	1.9013(5)	V(10)–O(16)	1.9727(6)	V(14)–O(22)	2.0523(9)
V(2)–O(21)	1.9582(7)	V(6)–O(24)	1.9119(6)	V(10)–O(18)	1.9875(5)	V(14)–O(19)	2.1726(6)
V(2)–O(19)	2.1004(7)	V(6)–O(29)	1.9362(8)	V(11)–O(11)	1.6106(6)	V(14)–O(39)	2.2933(7)
V(3)–O(3)	1.6128(5)	V(7)–O(7)	1.6120(6)	V(11)–O(21)	1.9550(7)	V(15)–O(15)	1.6086(6)
V(3)–O(24)	1.8818(6)	V(7)–O(18)	1.8918(6)	V(11)–O(26)	1.9587(6)	V(15)–O(34)	1.7950(6)
V(3)–O(23)	1.9030(7)	V(7)–O(32)	1.9180(7)	V(11)–O(36)	2.0175(7)	V(15)–O(36)	1.9276(6)
V(3)–O(25)	1.9305(8)	V(7)–O(28)	1.9656(7)	V(11)–O(33)	2.1063(7)	V(15)–O(30)	1.9311(7)
V(3)–O(22)	1.9915(6)	V(7)–O(27)	2.0033(8)	V(11)–O(38)	2.2616(8)	V(15)–O(31)	1.9546(5)
V(4)–O(4)	1.5686(6)	V(8)–O(8)	1.5917(4)	V(12)–O(12)	1.6305(7)		
V(4)–O(20)	1.7401(6)	V(8)–O(32)	1.9039(6)	V(12)–O(26)	1.9280(6)	C(1)–C(37)	1.2723(4)
V(4)–O(22)	1.9099(7)	V(8)–O(17)	1.9209(7)	V(12)–O(23)	1.9299(6)	C(1)–O(38)	1.3124(4)
V(4)–O(26)	1.9421(6)	V(8)–O(21)	1.9505(8)	V(12)–O(31)	1.9366(6)	C(1)–O(39)	1.2472(4)
V(4)–O(23)	1.9523(6)	V(8)–O(33)	2.0583(8)	V(12)–O(36)	1.9701(5)		
V(5)–O(5)	1.6231(5)	V(9)–O(9)	1.5880(4)	V(13)–O(13)	1.6192(4)		
O(1)–V(1)–O(16)	111.77(3)	O(5)–V(5)–O(30)	101.84(3)	O(4)–V(4)–O(22)	105.01(3)	O(37)–O(38)–O(39)	58.51(2)
O(1)–V(1)–O(17)	108.97(3)	O(5)–V(5)–O(37)	167.066(6)	O(4)–V(4)–O(23)	99.76(3)	O(37)–O(39)–O(38)	60.12(2)
O(1)–V(1)–O(18)	105.21(3)	O(27)–V(5)–O(28)	79.08(3)	O(4)–V(4)–O(26)	106.18(3)		
O(1)–V(1)–O(19)	106.92(3)	O(27)–V(5)–O(29)	102.16(3)	O(20)–V(4)–O(22)	95.26(3)	V(1)–O(16)–V(10)	98.79(2)
O(16)–V(1)–O(17)	138.93(2)	O(27)–V(5)–O(30)	156.02(1)	O(20)–V(4)–O(23)	156.57(1)	V(1)–O(16)–V(14)	102.17(3)
O(16)–V(1)–O(18)	81.68(2)	O(27)–V(5)–O(37)	72.86(3)	O(20)–V(4)–O(26)	94.58(2)	V(10)–O(16)–V(14)	134.11(2)
O(16)–V(1)–O(19)	81.89(3)	O(28)–V(5)–O(29)	157.907(9)	O(22)–V(4)–O(23)	79.89(3)	V(1)–O(17)–V(2)	104.11(3)
O(17)–V(1)–O(18)	92.71(3)	O(28)–V(5)–O(30)	92.29(3)	O(22)–V(4)–O(26)	143.94(2)	V(1)–O(17)–V(8)	144.92(1)
O(17)–V(1)–O(19)	81.67(3)	O(28)–V(5)–O(37)	88.71(2)	O(23)–V(4)–O(26)	77.42(2)	V(8)–O(17)–V(2)	95.07(3)
O(18)–V(1)–O(19)	147.47(2)	O(29)–V(5)–O(30)	77.67(3)	O(38)–C(1)–O(37)	117.97(2)	V(2)–O(20)–V(4)	128.77(2)
O(5)–V(5)–O(27)	101.83(3)	O(29)–V(5)–O(37)	70.97(2)	O(39)–C(1)–O(37)	119.71(2)	V(9)–O(34)–V(15)	128.86(2)
O(5)–V(5)–O(28)	102.02(2)	O(30)–V(5)–O(37)	84.72(3)	O(39)–C(1)–O(38)	122.32(2)		
O(5)–V(5)–O(29)	99.31(2)	O(4)–V(4)–O(20)	103.63(3)	O(38)–O(37)–O(39)	61.37(2)		

values for the O(19) and O(33) atoms imply considerable negative charge on the O atoms if they are not protonated. Since the bond orders for O(19) and O(33) are close to the value ($0.4 \times 3 = 1.2$) predicted for the four-co-ordinate OH^- in the crystal,[18] one proton can be located with a high degree of confidence on each of the O(19) and O(33) atoms. The significant lengthening of the V(1,2,14)–O(19) and V(8,9,11)–O(33) bond distances (average distances of 2.131 and 2.087 Å, respectively) is consistent with protonation of these sites. Furthermore, O(19)···O(39) and O(33)···O(38) distances are short at 2.6125(9) and 2.4995(7) Å, respectively (Table 3). Therefore, the small values of the bond orders for the O(19) and O(33) atoms suggest the involvement of a hydrogen-bonding proton between these oxygen atoms, although the hydrogen atoms could not be located directly from the three-dimensional X-ray diffraction data. Thus, the co-ordination of two hydrogen atoms in the anion enables us to formulate the complex $K_5H_2[V_{15}O_{36}(CO_3)]$ as $K_5[V_{15}O_{34}(OH)_2(CO_3)]$, the hydrogen atoms participating in the stabilization of CO_3^{2-} at the central cavity by hydrogen bonding.

Fig. 4 illustrates the packing of complex **1** in the crystal. If a maximum K–O distance of 3.27 Å is assumed, K–O distances for the potassium–oxygen polyhedra are 2.6750(8)–3.269(1) Å (Table 3). The K^+ cations occupy positions between the anions in irregular seven- to nine-co-ordination with oxygen: the oxygen co-ordination to K(1), K(2) and K(4) is nine-fold and eight- and seven-fold to K(3) and K(5), respectively. Cations and water molecules serve to bind the anions together by a complex system of ionic and hydrogen bonds. In the structure determination of complex **1** the site occupancies of the lattice waters O(49)–O(59) are fixed at 0.5 throughout the structure refinements, since, except for the O(52) and O(54) atoms, the distances between these oxygen atoms is very short (< 2.3 Å) which may be brought about by the disordered structure of these atoms and the fixing of the site occupancies of O(52) and O(54) at 1 giving rise to non-convergence of some solvent water through the refinement.

CIDEP at Room Temperature and Solution Photochemistry.—Fig. 5 shows the CIDEP spectra at various time delays after the laser excitation of the $[V_4O_{12}]^{4-}$–MeOH system at pH 9 (adjusted using K_2CO_3). The observed spectra at $g = 2.001$ show 1:2:1 triplet hyperfine structures (with an equal splitting of $a_{\alpha\text{-H}} = 1.76 \pm 0.03$ mT) with total emissive CIDEP signals within the first 2 μs after the laser pulse. The hyperfine structure is similar to that of the continuous-wave ESR spectrum of $\dot{C}H_2OH$ with three peaks of intensity 1:2:1 corresponding to the two equivalent $I = \frac{1}{2}$ spin states of the hydrogen atoms.[19] Therefore, the observed time-resolved ESR spectra are attributed to $\dot{C}H_2OH$ radicals. Traces of the emissive CIDEP signals of $\dot{C}H_2OH$ were not evident in the absence of $[V_4O_{12}]^{4-}$. The spectra were obtained at a microwave power of 10–40 mW and at concentrations of 8×10^{-2} and $> 10^{-1}$ mol dm^{-3} $[V_4O_{12}]^{4-}$ and MeOH, respectively. Variation of the solution pH level induced little change in the g or $a_{\alpha\text{-H}}$ values, but there was a significant change in the signal intensity. Fig. 6 shows the emissive signal intensity of the central hyperfine component at 0.5 μs after the exciting laser pulse as a function of solution pH ranging from 5 to 11. The pH dependence of the signal intensity exhibiting its optimum around 9 bears a striking resemblance to that of the yield of photoinduced H_2, indicating that the formation of $\dot{C}H_2OH$ reflects the H_2 formation. The continuous-wave ESR spectrum of the photolyte after the laser pulse irradiation (also in Fig. 6) showed the presence of a paramagnetic species (with $g = 1.972$ and $a_V = 9.72$–9.80 mT) at room temperature. A similar continuous-wave ESR signal ($\langle g \rangle = 1.973$ and $\langle a_V \rangle = 9.78$ mT) was obtained for the UV-irradiated $[NH_3Bu^t]_4[V_4O_{12}]$ single crystal which implied the formation of the localized $V^{IV}O_3(OH)$ centre in a manner similar to that of alkylammonium polyoxo-

Table 3 Selected interatomic distances (Å) and angles (°) for complex **1** with e.s.d.s in parentheses*

K(1)···O(2)	3.139(1)	K(4)···O(6^{VI})	3.061(1)	O(44)···O(41^{II})	2.786(1)	O(56)···O(59)	1.2509(3)
K(1)···O(2^{I})	2.889(1)	K(4)···O(12^{VI})	3.1244(9)	O(46)···O(52^{VIII})	2.6754(8)	O(56)···O(58^{XIV})	2.2950(7)
K(1)···O(7^{II})	2.746(1)	K(4)···O(14)	2.8132(9)	O(46)···O(22^{III})	2.7897(8)	V(1)···V(3)	5.589(2)
K(1)···O(8)	2.937(1)	K(4)···O(15^{VI})	3.208(1)	O(47)···O(27^{II})	2.781(1)	V(1)···V(7)	3.655(1)
K(1)···O(17)	2.7702(9)	K(4)···O(31^{VI})	2.811(1)	O(48)···O(29^{IX})	2.7595(8)	V(1)···V(8)	3.643(1)
K(1)···O(42)	2.7734(8)	K(4)···O(45^{I})	2.878(1)	O(48)···O(48^{IX})	2.793(1)	V(2)···V(4)	3.316(1)
K(1)···O(47)	2.8059(7)	K(4)···O(46^{VI})	2.9356(8)	O(50)···O(51^{XI})	2.7500(8)	V(2)···V(9)	5.373(2)
K(1)···O(56)	2.838(1)	K(4)···O(52^{I})	3.204(1)	O(50)···O(6^{IX})	2.7674(8)	V(2)···V(10)	5.443(2)
K(1)···O(59)	3.081(1)	K(5)···O(2^{I})	2.8834(9)	O(52)···O(54^{II})	2.6593(8)	V(3)···V(6)	3.641(1)
K(2)···O(1)	2.962(1)	K(5)···O(8)	2.6750(8)	O(52)···O(46^{XIII})	2.6754(8)	V(3)···V(12)	3.653(1)
K(2)···O(7)	3.116(1)	K(5)···O(15^{VII})	2.982(1)	O(53)···O(40^{IV})	2.7697(7)	V(4)···V(13)	5.363(2)
K(2)···O(7^{II})	3.235(1)	K(5)···O(36^{VII})	2.807(1)	O(53)···O(6^{VI})	2.7754(9)	V(4)···V(15)	5.420(2)
K(2)···O(8^{II})	2.906(1)	K(5)···O(42^{I})	2.983(1)	O(51)···O(54)	2.480(1)	V(5)···V(11)	5.703(2)
K(2)···O(9^{II})	3.187(1)	K(5)···O(45)	2.8462(9)	O(51)···O(51^{XI})	2.5735(7)	V(5)···V(14)	5.659(2)
K(2)···O(10)	3.0795(8)	K(5)···O(47)	3.269(1)	O(51)···O(35)	2.6828(9)	V(6)···V(7)	5.522(2)
K(2)···O(18)	2.724(1)	O(19)···O(39)	2.6125(9)	O(54)···O(10)	2.7321(8)	V(6)···V(12)	3.673(1)
K(2)···O(32^{II})	2.7292(8)	O(33)···O(38)	2.4995(7)	O(55)···O(5^{II})	2.5913(8)	V(7)···V(8)	3.676(1)
K(2)···O(57)	2.853(1)	O(37)···O(39)	2.1787(1)	O(55)···O(56)	2.6997(8)	V(8)···V(12)	5.536(2)
K(3)···O(3)	3.0884(9)	O(37)···O(38)	2.2153(8)	O(59)···O(9^{VI})	2.7498(9)	V(9)···V(10)	5.309(2)
K(3)···O(4^{III})	3.883(1)	O(38)···O(39)	2.2424(7)	O(49)···O(51^{I})	1.2720(4)	V(9)···V(15)	3.340(1)
K(3)···O(6)	3.2059(9)	O(20)···O(34)	6.798(2)	O(49)···O(50^{X})	1.7144(5)	V(10)···V(13)	3.314(1)
K(3)···O(12^{III})	3.0931(9)	O(20)···O(35)	6.762(2)	O(49)···O(53^{I})	1.9150(6)	V(11)···V(14)	5.682(2)
K(3)···O(13)	3.015(1)	O(34)···O(35)	6.713(2)	O(50)···O(53^{XI})	0.4605(5)	V(13)···V(15)	5.361(2)
K(3)···O(23^{III})	2.752(1)	O(41)···O(44^{II})	2.786(1)	O(50)···O(49^{XII})	1.7144(5)	V(5)···O(20)	7.204(2)
K(3)···O(24)	2.7648(8)	O(43)···O(59)	2.6285(8)	O(55)···O(58^{XIV})	0.9137(4)	V(11)···O(35)	7.165(3)
K(3)···O(41^{IV})	3.062(1)	O(43)···O(1)	2.662(1)	O(55)···O(57^{XIV})	2.2636(8)	V(14)···O(34)	7.174(2)
K(4)···O(3^{V})	2.7988(8)	O(44)···O(49^{I})	2.6979(8)				

V(7)···V(1)···V(8)	60.48(2)	V(1)···V(7)···V(8)	59.60(2)	O(34)···O(20)···O(35)	59.35(2)
V(9)···V(2)···V(10)	58.79(2)	V(2)···V(9)···V(10)	61.26(2)	O(20)···O(34)···O(35)	60.05(2)
V(6)···V(3)···V(12)	60.47(2)	V(5)···V(11)···V(14)	59.61(2)	V(3)···V(1)···V(7)	89.65(3)
V(13)···V(4)···V(15)	59.63(2)	V(4)···V(13)···V(15)	60.71(2)	V(3)···V(1)···V(8)	89.36(3)
V(11)···V(5)···V(14)	60.01(2)	O(38)···O(37)···O(39)	61.37(2)	V(4)···V(2)···V(9)	91.06(3)
V(3)···V(6)···V(12)	59.93(2)	O(37)···O(38)···O(39)	58.51(2)	V(4)···V(2)···V(10)	88.35(3)

* Symmetry codes: I $-x, 1-y, 1-z$; II $1-x, 1-y, 1-z$; III $-x, -y, -z$; IV $x, -1+y, z$; V $-x, -y, 1-z$; VI $x, y, 1+z$; VII $-x, 1-y, -z$; VIII $x, -1+y, -1+z$; IX $1-x, -y, -z$; X $-1+x, 1+y, z$; XI $1-x, -y, 1-z$; XII $1+x, -1+y, z$; XIII $x, 1+y, 1+z$; XIV $1-x, 1-y, 2-z$. The site occupancies of the O(49)–O(59) atoms are fixed at 0.5 throughout the structure refinements.

Table 4 Sum of the vanadium–oxygen bond strengths about given atoms*

	a	b		a	b		a	b
V(1)	4.3(2)	4.1(2)	O(3)	1.7(1)	1.6(1)	O(20)	1.9(1)	1.8(1)
V(2)	4.3(2)	4.0(2)	O(4)	1.8(1)	1.7(1)	O(21)	1.9(1)	1.8(1)
V(3)	4.4(1)	4.2(1)	O(5)	1.8(1)	1.7(1)	O(22)	1.8(1)	1.8(1)
V(4)	5.2(2)	4.9(2)	O(6)	1.7(1)	1.6(1)	O(23)	2.2(1)	1.9(1)
V(5)	4.3(2)	4.1(2)	O(7)	1.8(1)	1.7(1)	O(24)	2.1(1)	2.0(1)
V(6)	4.7(2)	4.4(2)	O(8)	1.7(1)	1.6(1)	O(25)	2.0(1)	1.8(1)
V(7)	4.5(2)	4.2(2)	O(9)	1.8(1)	1.7(1)	O(26)	2.0(1)	1.8(1)
V(8)	4.4(2)	4.1(2)	O(10)	1.7(1)	1.6(1)	O(27)	1.8(1)	1.7(1)
V(9)	4.5(2)	4.2(2)	O(11)	1.7(1)	1.6(1)	O(28)	1.9(1)	1.8(1)
V(10)	4.6(2)	4.3(2)	O(12)	1.5(1)	1.4(1)	O(29)	1.9(1)	1.8(1)
V(11)	4.4(2)	4.1(2)	O(13)	1.8(1)	1.7(1)	O(30)	2.0(1)	1.8(1)
V(12)	4.2(2)	3.9(2)	O(14)	1.8(1)	1.7(1)	O(31)	2.1(1)	1.9(1)
V(13)	4.7(2)	4.4(2)	O(15)	1.7(1)	1.7(1)	O(32)	2.1(1)	1.9(1)
V(14)	4.2(2)	3.9(2)	O(16)	1.9(1)	1.8(1)	O(33)	1.4(1)	1.3(1)
V(15)	4.7(2)	4.4(2)	O(17)	2.1(1)	1.9(1)	O(34)	1.7(1)	1.6(1)
O(1)	1.8(1)	1.7(1)	O(18)	2.1(1)	1.9(1)	O(35)	1.7(1)	1.6(1)
O(2)	1.7(1)	1.6(1)	O(19)	1.2(1)	1.1(1)	O(36)	1.8(1)	1.7(1)

* The sums a and b are calculated using the expressions $\Sigma[d(V^{V}\text{–}O)/1.791]^{-5.1}$ and $\Sigma[d(V^{IV}\text{–}O)/1.770]^{-5.2}$, respectively.

molybdate lattices (data not shown).[20] The formation of two localized paramagnetic V^{IV} centres in the $[NH_3Bu^t]_4[V_4O_{12}]$ lattice is possible if the crystal has a space group of $I4/m$ and $Z = 2$.[6] Thus, the paramagnetic species ($g = 1.972, a_V = 9.72$–9.80 mT) in the photolyte can be assigned to $[V_4O_{12}H]^{4-}$ (one-electron reduction species) or $[V_4O_{12}H_2]^{4-}$ (two-electron reduction species).

The observed polarization of the $\dot{C}H_2OH$ radical is mainly interpreted by the triplet mechanism originating from the O ⟶ V l.m.c.t. excited triplet states ($^3[V_4O_{12}]^{4-}$) of $[V_4O_{12}]^{4-}$, as discussed below: these excited states react with MeOH *via* hydrogen abstraction to yield $[V_4O_{12}H]^{4-}$ and $\dot{C}H_2OH$ radicals. The former will be converted to either $[V_4O_{12}]^{4-}$ with accompanying H_2 formation or $[V_{15}O_{36}(CO_3)]^{7-}$ encapsulating CO_3^{2-}. The observed photolysis of $[V_4O_{12}]^{4-}$ in the presence of MeOH can be represented by equations (1)–(6). The $\dot{C}H_2OH$ radical will readily reduce

$$[V_4O_{12}]^{4-} \xrightarrow{h\nu} {}^3[V_4O_{12}]^{4-} \quad (1)$$

$$^3[V_4O_{12}]^{4-} + MeOH \longrightarrow [V_4O_{12}H]^{4-} + \dot{C}H_2OH \quad (2)$$

$$[V_4O_{12}H]^{4-} \longrightarrow [V_4O_{12}]^{4-} + \tfrac{1}{2}H_2 \quad (3)$$

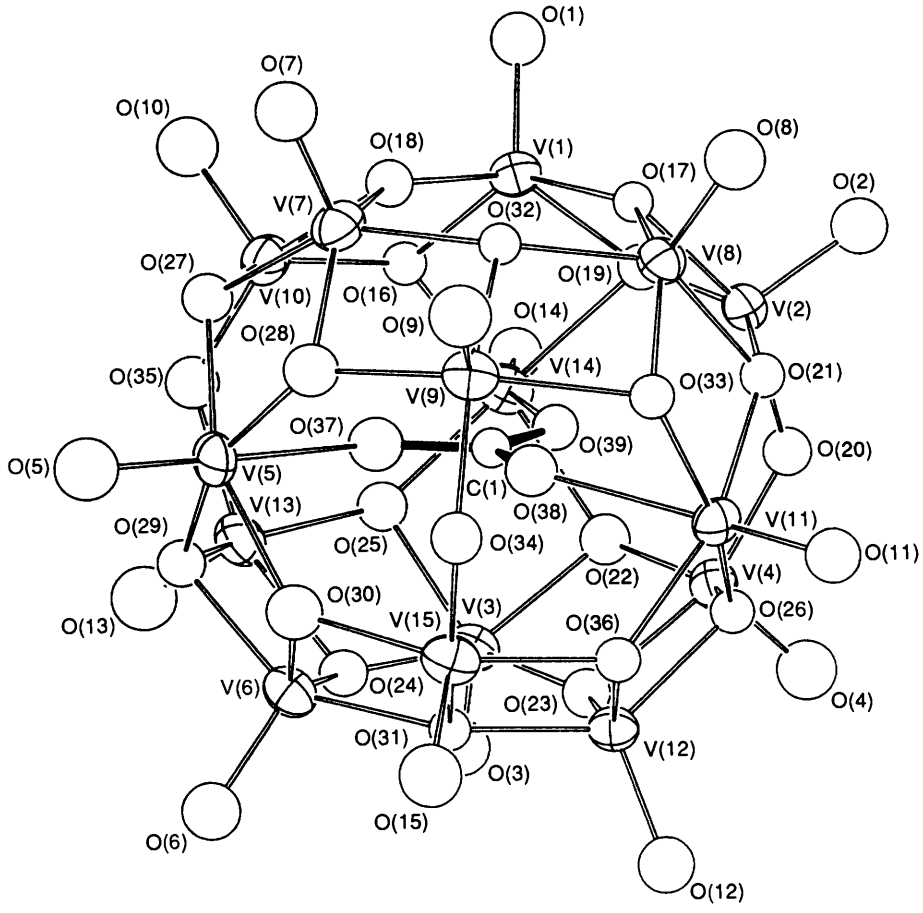

Fig. 2 Schematic representation of the structure of the $[V_{15}O_{36}(CO_3)]^{7-}$ anion with atom labelling

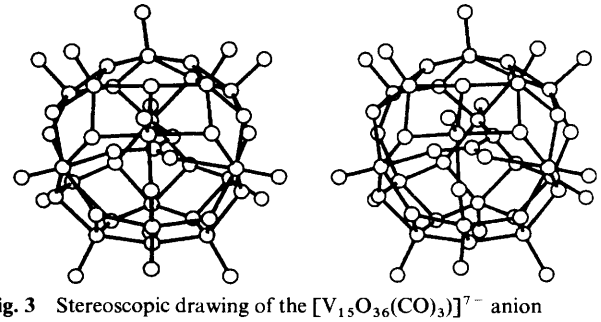

Fig. 3 Stereoscopic drawing of the $[V_{15}O_{36}(CO)_3)]^{7-}$ anion

$$[V_4O_{12}]^{4-} + \dot{C}H_2OH \longrightarrow [V_4O_{12}H]^{4-} + HCHO \quad (4)$$

$$[V_4O_{12}H]^{4-} + \dot{C}H_2OH \longrightarrow [V_4O_{12}H_2]^{4-} + HCHO \quad (5)$$

$$4[V_4O_{12}H_2]^{4-} + CO_3^{2-} \rightleftharpoons [V_{15}O_{36}(CO_3)]^{7-} + VO_4^{3-} + 8OH^- \quad (6)$$

$[V_4O_{12}]^{4-}$ and $[V_4O_{12}H]^{4-}$ at a rate close to the diffusion limit due to its highly negative half-wave potential ($E_{\frac{1}{2}} = -1.1$ V *vs.* Ag–AgCl),[21] as denoted by equations (4) and (5). Such an exoergonic reaction of $\dot{C}H_2OH$ in the photochemistry of polyoxometalates has been discussed previously.[22,23] The formation of complex **1** led to an increase ($\Delta pH \approx 1$) in pH of the photolyte. This let us propose the liberation of monomeric VO_4^{3-} and OH^- from $[V_4O_{12}H_2]^{4-}$ for the formation of $[V_{15}O_{36}(CO_3)]^{7-}$, as shown by equation (6). Thus, the overall reaction for the formation of $[V_{15}O_{36}(CO_3)]^{7-}$ can be represented by equation (7), although the stoichiometry of the reaction is not clarified at present.

$$4[V_4O_{12}]^{4-} + CO_3^{2-} + 4MeOH \xrightarrow{h\nu} [V_{15}O_{36}(CO_3)]^{7-} + VO_4^{3-} + 8OH^- + 4HCHO \quad (7)$$

For such a mechanism to occur, the triplet O ⟶ V l.m.c.t. state should react with MeOH faster than the spin-lattice relaxation time in the solution phase. We could not observe a CIDEP signal of the counterpart species, probably because of the short spin-lattice relaxation time of $[V_4O_{12}H]^{4-}$ compared to $\dot{C}H_2OH$. Fig. 5 also shows CIDEP signals obtained with different delay times. The ratio of the signal intensities of three hyperfine peaks does not change in all gate times and hence it is concluded that the magnetic relaxation time has no effect on the ratio of the CIDEP signal intensities. It is noteworthy that the broadening of the CIDEP signals occurs at the early stages after laser pulse irradiation: each of the triplet hyperfine lines at 0.68 μs after the laser pulse is split into a doublet with equal spacing of 0.06 mT due to an OH proton of $\dot{C}H_2OH$, as shown in Fig. 5.

We measured the CIDEP for the $[V_4O_{12}]^{4-}$–EtOH or –Pr^{i}OH system at pH 9. The results are shown in Fig. 7, where the emissive signals having intensity ratios of 1:1:3:3:3:1:1 and 1:6:15:20:15:6:1 can be attributed to MeĊHOH ($g = 2.003$, $a_{\alpha\text{-H}} = 1.50$ mT, $a_{\beta\text{-H}} = 2.25$ mT) and $Me_2\dot{C}OH$ ($g = 2.001$, $a_{\beta\text{-H}} = 2.00$ mT), respectively. Similar parameters were obtained for the continuous-wave ESR spectra of MeĊHOH and $Me_2\dot{C}OH$ radicals.[19] The formation of these two radicals confirms the involvement of α-hydrogen abstraction from alcohols in the photoredox reaction between the O ⟶ V l.m.c.t. excited triplet of $[V_4O_{12}]^{4-}$ and alcohols.

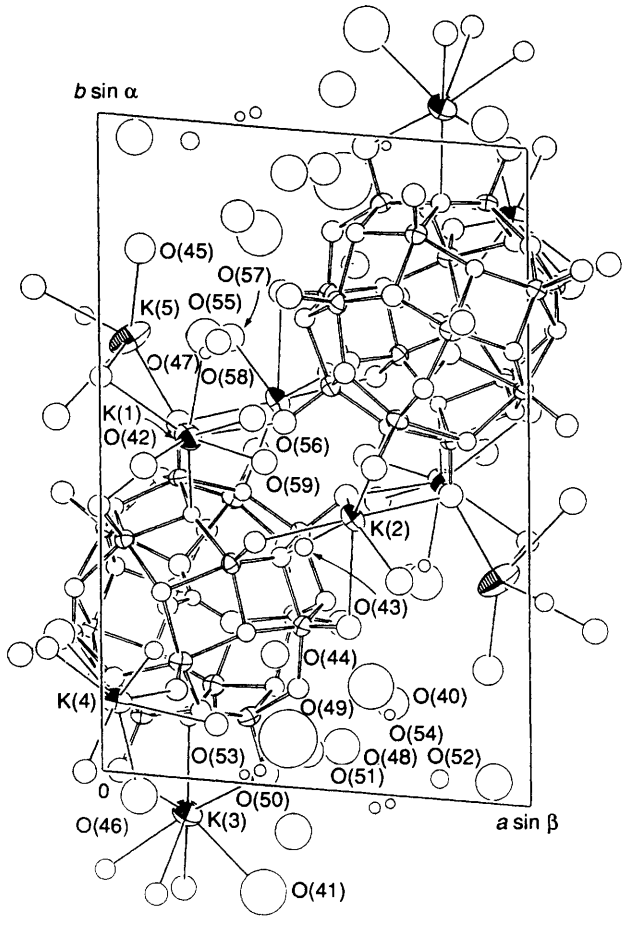

Fig. 4 Packing diagram of complex **1** viewed along the *c* axis

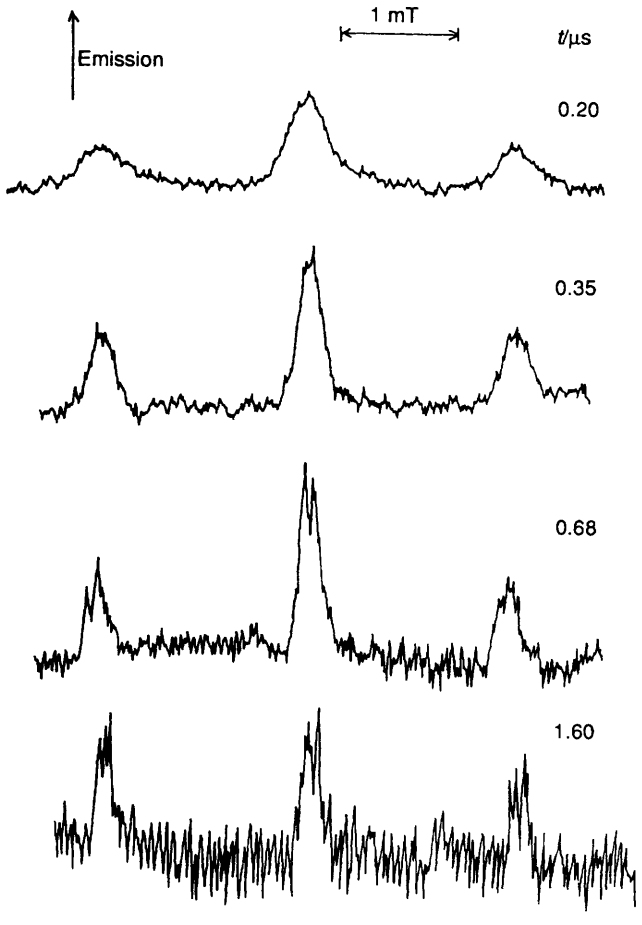

Fig. 5 Time-resolved ESR spectra taken at the delay times indicated during the photolysis of the $[V_4O_{12}]^{4-}$–MeOH system at pH 9 at room temperature

The emissive CIDEP spectra of α-hydroxyalkyl radicals are also observed for other polyoxometalates such as $[Mo_7O_{24}]^{6-}$ and $[W_{10}O_{32}]^{4-}$ in the presence of MeOH (0.9 mol dm^{-3}), as shown in Fig. 8. The spectral shape (g = 2.004, $a_{\alpha\text{-H}}$ = 1.78 mT) for the $[W_{10}O_{32}]^{4-}$ system in acetonitrile was similar to that (g = 2.004, $a_{\alpha\text{-H}}$ = 1.75 mT) for the $[Mo_7O_{24}]^{6-}$ system in water but the signal intensity for the $[W_{10}O_{32}]^{4-}$ system decreased significantly, in contrast to those for other polyoxometalate systems [Figs. 5 and 8(*a*)]. Such a reduction cannot be attributed to a decrease in absorption of the exciting laser light, since the absorption coefficient at 308 nm for $[W_{10}O_{32}]^{4-}$ (ε = 7.2 × 10^3 dm^3 mol^{-1} cm^{-1} in MeCN) is larger than for other polyoxometalates (ε = 3.6 × 10^3 and 1.8 × 10^3 dm^3 mol^{-1} cm^{-1} for $[V_4O_{12}]^{4-}$ and $[Mo_7O_{24}]^{6-}$ in water, respectively), suggesting that the electron transfer between the triplet O ⟶ W l.m.c.t. state and MeOH is slow to generate the polarized $\dot{C}H_2OH$ radical.

The above results show that polyoxometalates are good sensitizers for obtaining polarized α-hydroxyalkyl radicals, which would be useful in studying radical chemistry using the time-resolved ESR technique.

Discussion

Structure of the $[V_{15}O_{36}(CO_3)]^{7-}$ *Anion.*—As can be seen from the V–O distances and the O–V–O angles (Table 2) the VO_5 tetragonal pyramids and VO_6 octahedra are all distorted. The nearly spherical $V_{15}O_{36}$ cluster shell exhibits V–O distances varying from 1.5686(6) to 2.1726(6) Å; 1.5686(6)–1.6305(7) for the O(1)–O(15) terminal oxygens, 1.7401(6)–1.9362(8) for the O(20), O(34) and O(35) two-co-ordinate oxygens and 1.8818(6)–2.1726(6) Å for the other three-co-ordinate oxygens. The vanadium framework in the anion is

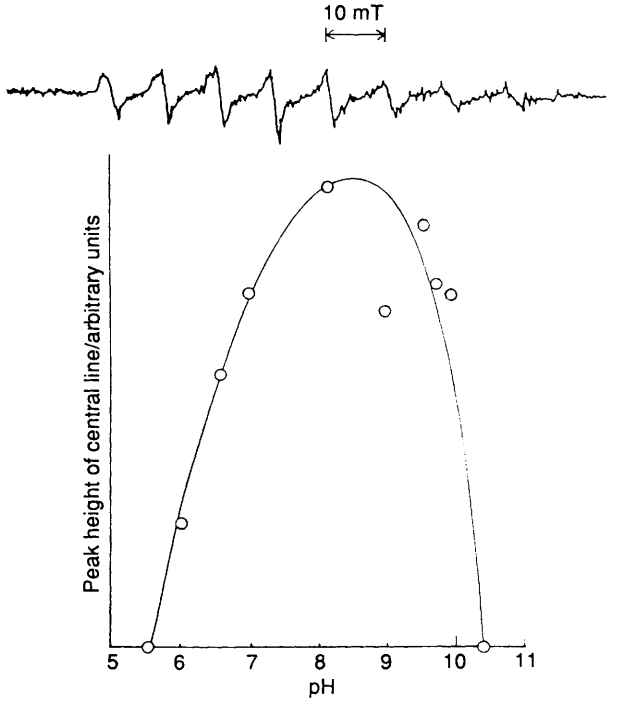

Fig. 6 Solution pH dependence of the total nuclear-spin quantum number (M = 0) peak in the CIDEP spectrum of $\dot{C}H_2OH$ after a time delay of 0.5 μs. The continuous-wave ESR spectrum is for the photolyte after the CIDEP measurement

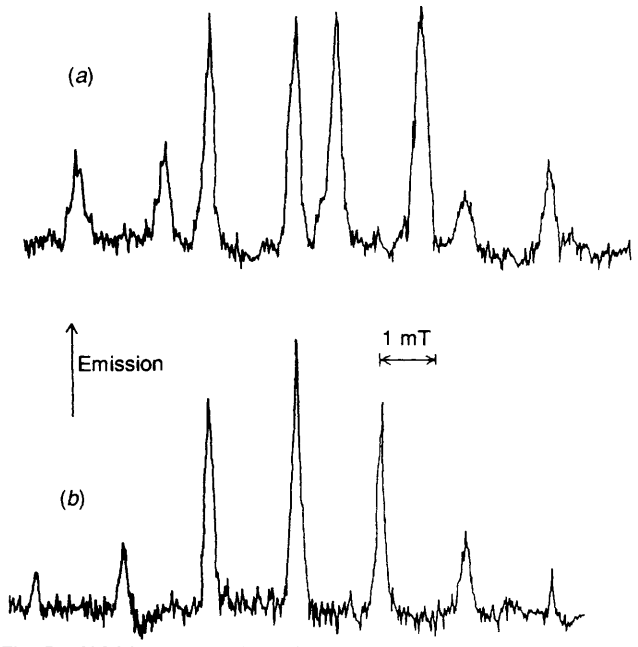

Fig. 7 CIDEP spectra taken after a time delay of 0.5 μs during the photolysis of the $[V_4O_{12}]^{4-}$–EtOH (*a*) and $[V_4O_{12}]^{4-}$–Pr^{i}OH (*b*) systems at pH 9

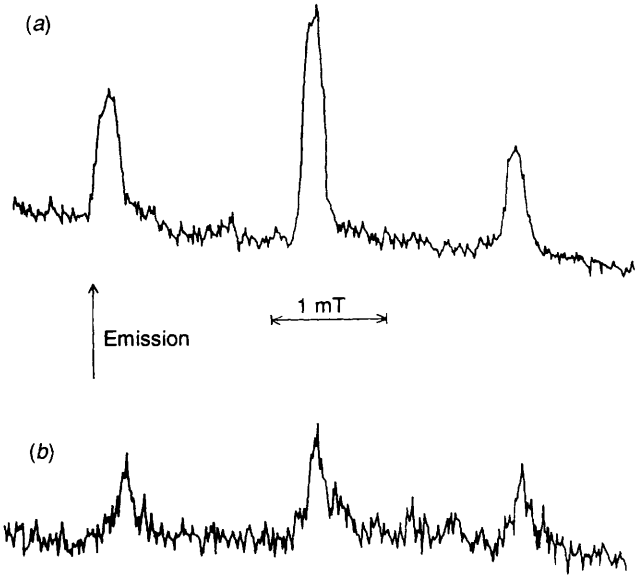

Fig. 8 CIDEP spectra taken after a time delay of 0.5 μs during the photolysis of the $[Mo_7O_{24}]^{6-}$–MeOH (at pH 6) (*a*) and $[W_{10}O_{32}]^{4-}$–MeOH (*b*) systems in MeCN

shown in Fig. 9. The anion consists of five triangle planes of vanadium atoms with V–V–V almost 60° for each triangle (Table 3) and shows D_{3h} symmetry in two nearly equally weighted orientations related by the V(5,11,14) mirror plane. The CO_3^{2-} carbon atom is approximately located midway between the centre of the V(15,11,14) and O(37,38,39) triangles at distances of 0.129 and 0.002 Å from the V(5,11,14) and O(37,38,39) (O–O–O almost 60°) triangle planes, respectively. The seven triangle planes of V, CO_3^{2-} O, and two-co-ordinated O(20,34,35) atoms are almost parallel to each other. Table 5 shows the dihedral angles between the seven triangle planes within the molecule. The triangle plane composed of the two-co-ordinated oxygen atoms, O(20,34,35) [average O···O 6.758(2) Å, O–O–O almost 60°], is located 0.004 Å below the central V(5,11,14) triangle plane with 60° rotation. The σ_h V(5,11,14) triangle plane [average V···V 5.681(2) Å] brings each belt vanadium atom of the V(4,13,15) triangle plane

Table 5 Dihedral angles (°) between planes*

Plane	1	2	3	4	5	6
2	178.65					
3	0.65	178.55				
4	1.13	179.68	1.36			
5	1.12	178.95	0.70	1.13		
6	6.55	174.49	6.90	5.54	6.55	
7	179.23	1.37	179.83	178.68	179.46	173.14

* Plane 1, V(1)V(7)V(8); 2, V(2)V(9)V(10); 3, V(5)V(11)V(14); 4, V(4)V(13)V(15); 5, V(3)V(6)V(12); 6, O(37)O(38)O(39); 7, O(20)O(34)O(35).

[average V···V 5.381(2) Å] into near coincidence with an atom of another belt, to give 'composite' belt atoms of the V(2,9,10) plane with an average V···V distance of 5.375(2) Å. Two belt triangle planes undergo 60° rotations. The apparent distances for the V(2,9,10) and V(4,13,15) planes from the central V(5,11,14) plane are 1.701 and 1.621 Å, respectively. The O(37,38,39) plane is located 0.091 Å towards the V(2,9,10) plane at a point equidistant (1.661 Å) from the V(2,9,10) and V(4,13,15) planes. This may be associated with the presence of the hydrogen bonding of the CO_3^{2-} O(39) and O(38) atoms with the O(19) and O(33) atoms, which co-ordinate the V(1,2,14) and V(8,9,11) atoms, respectively (Tables 3 and 4). The V(1,7,8) triangle polar plane [average V···V 3.658(1) Å] is 5.549 Å distant from the other triangle polar plane, V(3,6,12), average V···V 3.656(2) Å. The distance (5.549 Å) between the two V(1,7,8) and V(3,6,12) triangle planes is significantly shorter than the average value (7.181 Å) of the V(5)···O(20), V(11)···O(35) and V(14)···O(34) distances [7.204(2), 7.165(2) and 7.174(2) Å, respectively] which corresponds to the diameter of the approximately equatorial V(5)O(34)V(11)-O(20)V(14)O(35) circle. This indicates a significant distortion of the $[V_{15}O_{36}(CO_3)]^{7-}$ cluster shell from a perfect sphere.

Electron Transfer from the O ⟶ M *l.m.c.t. Triplet State.*—Intramolecular transfer of the O ⟶ M l.m.c.t. triplet excitation energy has been revealed by measurements of the luminescence of the O ⟶ M l.m.c.t. triplet states for a variety of polyoxometalate solids of tungsten and molybdenum.[4] The difficulty in observing the luminescence from the O ⟶ M l.m.c.t. triplet states in aqueous solutions can be explained by the strong effect of the hydrogen-bonding network between the anions on the non-radiative deactivation of the O ⟶ M l.m.c.t. excited states, due to the electrostatic dipole–dipole interaction at the MO_6 octahedra with a resultant decrease in both the quantum yield and the lifetime of the luminescence.[4] Therefore, the polarization signal of the α-hydroxyalkyl radical for the $[V_4O_{12}]^{4-}$–alcohol system in aqueous solutions is informative for the determination of the reaction precursor, the O ⟶ V l.m.c.t. singlet or triplet state. In the triplet mechanism, the intensity ratio of the polarization signal is the same as the statistical ratio (1:2:1 in $\dot{C}H_2OH$), whereas it is dependent on the nature of the radical pair in the case of the radical-pair mechanism.[8–10] This latter mechanism would give rise to an asymmetric spectrum, although all the signal lines of $\dot{C}H_2OH$ become emissive due to the large differences in *g* and the hyperfine coupling constant between the two radicals of $\dot{C}H_2OH$ (g = 2.001–2.004 and $a_{\alpha\text{-H}}$ = 1.74–1.79 mT) and $[V_4O_{12}H]^{4-}$ (g = 1.972 and a_V = 9.72–9.80 mT).[24,25] The polarization due to the radical-pair mechanism has often been observed in the viscous Pr^{i}OH (η = 1.765 at 30 °C) system.[26] However, the absence of an asymmetric pattern for the CIDEP signals for the $[V_4O_{12}]^{4-}$– and $[Mo_7O_{24}]^{6-}$–alcohol systems in water and the $[W_{10}O_{32}]^{4-}$–MeOH system in MeCN (Figs. 5–8) strongly supports the predominance of the triplet over the radical-pair mechanism. Consequently, the reaction precursor for the α-hydroxyalkyl radical formation is the O ⟶ M

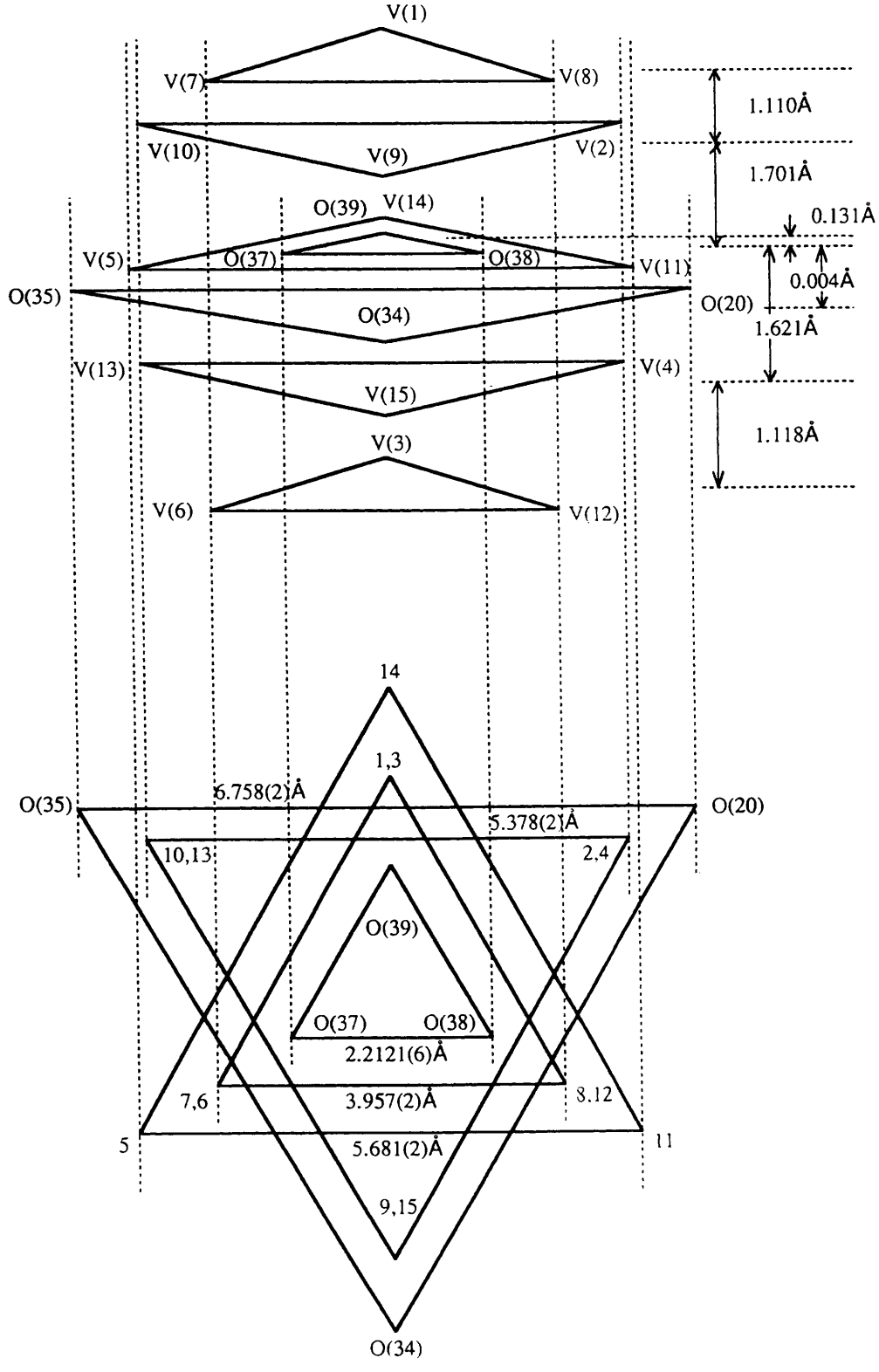

Fig. 9 Vanadium framework of the anion for complex **1**. The average distance (Å) between the two triangle planes was estimated based on the distance between the central carbon atom and the triangle plane

l.m.c.t. triplet state of the polyoxometalates, as denoted by equation (2): the possibility of the involvement of the O ⟶ V l.m.c.t. excited singlet state in the $\dot{C}H_2OH$ radical formation, which would provide the polarized radical pair, can be excluded. The lifetime of the O ⟶ M l.m.c.t. triplet states at room temperature in aqueous solutions should be much shorter than 100 μs, the lifetime at 100 K in the solid state.[4] The decay rate of the polarization of the $\dot{C}H_2OH$ radical for $[V_4O_{12}]^{4-}$ in water was estimated to be approximately $(0.9\ \mu s)^{-1}$ (Fig. 5). A similar result was obtained for $[Mo_7O_{24}]^{6-}$ and $[W_{10}O_{32}]^{4-}$. Since the decay of the spin polarization of $\dot{C}H_2OH$ is similar to the electron-spin relaxation time (0.6 μs) of the $\dot{C}H_2OH$ radical generated by pulse radiolysis of an N_2O-saturated aqueous methanolic solution at pH 7,[24] it is implied that the electron-

spin relaxation of the α-hydroxyalkyl radical is the main process terminating the polarization in the present systems. Then, an observable reduction in the signal intensity for the EtOH or Pr^iOH system compared with the MeOH system suggests that the redox reaction of the O ⟶ V l.m.c.t. excited triplet state of $[V_4O_{12}]^{4-}$ with EtOH or Pr^iOH occurs more slowly than with MeOH.

If the linewidth is determined in part by the unresolved electron spin–spin exchange interaction in the $[V_4O_{12}H]^{4-} \cdots \dot{C}H_2OH$ radical pair, the gradual reduction in apparent linewidth with an accompanying resolution of the hydroxy proton coupling for $\dot{C}H_2OH$ in the time domain from 0.2 to 1.6 μs (Fig. 5) would be attributed to an increase in the average distance between the radicals forming the pair, reflecting the extinction of the exchange interaction.[25] However, the absence of distortion of the ESR polarization of the $\dot{C}H_2OH$ radical and the absence of the external magnetic field effect indicate that the interaction between $[V_4O_{12}H]^{4-}$ and the $\dot{C}H_2OH$ radicals is extremely weak in water, resulting in little probability of signal decay through back electron transfer from $[V_4O_{12}H]^{4-}$ to $\dot{C}H_2OH$. Little contribution of $[V_4O_{12}H]^{4-}$ to the observed time-resolved spectrum leads to the conclusion that the spin-lattice relaxation of $[V_4O_{12}H]^{4-}$ is faster than that of the α-hydroxyalkyl radicals.

References

1 T. Yamase and R. Watanabe, *Inorg. Chim. Acta*, 1983, **77**, L193.
2 D. Rehder, *Bull. Magn. Reson.*, 1982, **4**, 33.
3 L. Pettersson, B. Hedman, I. Anderson and N. Ingri, *Chem. Scr.*, 1983, **22**, 254.
4 T. Yamase and M. Sugeta, *J. Chem. Soc., Dalton Trans.*, 1993, 759.
5 J. Fuchs, S. Mahjour and J. Pickardt, *Angew. Chem., Int. Ed. Engl.*, 1976, **15**, 374.
6 P. Román, A. San José, A Luque and J. M. Gutiérrez-Zorrilla, *Inorg. Chem.*, 1993, **32**, 775.
7 A. Müller, M. Penk, R. Rohlfing, E. Krickemeyer and K. J. Döring, *Angew. Chem., Int. Ed. Engl.*, 1990, **29**, 926.
8 L. T. Muss, P. W. Atkins, K. A. McLauchlan and J. B. Pedersen, *Chemically Induced Magnetic Polarization*, Reidel, Dordrecht, 1977; F. J. Adrian, *Rev. Chem. Intermed.*, 1979, **3**, 3.
9 P. J. Hore, C. G. Joshin and K. A. McLauchlan, *Chem. Soc. Rev.*, 1979, **8**, 29.
10 S. K. Wong, D. A. Hutchison and J. K. S. Wan, *J. Chem. Phys.*, 1973, **59**, 985.
11 M. Filowitz, R. K. C. Ho, W. G. Klemperer and W. Shum, *Inorg. Chem.*, 1979, **18**, 93; T. Yamase, N. Takabayashi and M. Kaji, *J. Chem. Soc., Dalton Trans.*, 1981, 628.
12 G. K. Johnson and E. O. Schlemper, *J. Am. Chem. Soc.*, 1978, **100**, 3645.
13 G. J. Gilmore, *J. Appl. Crystallogr.*, 1984, **42**, 46.
14 N. Walker and D. Stuart, *Acta Crystallogr., Sect. A*, 1983, **158**, 3.
15 TEXSAN, Single-crystal structure analysis software, Molecular Structure Corporation, The Woodlands, TX, 1989.
16 I. D. Brown and K. K. Wu, *Acta Crystallogr., Sect. B*, 1976, **32**, 1957.
17 D. Altermatt and I. D. Brown, *Acta Crystallogr., Sect. B*, 1985, **41**, 240; I. D. Brown and D. Altermatt, *Acta Crystallogr., Sect. B*, 1985, **41**, 144.
18 J. Emsley, *Chem. Soc. Rev.*, 1980, **9**, 91.
19 P. Livingston and H. Zeldes, *J. Chem. Phys.*, 1966, **44**, 1245.
20 T. Yamase and M. Suga, *J. Chem. Soc., Dalton Trans.*, 1989, 661; T. Yamase, *J. Chem. Soc., Dalton Trans.*, 1985, 2585; 1982, 1987; *Polyhedron*, 1986, **5**, 79.
21 J. Lilie, G. Beck and A. Henglein, *Ber. Bunsenges. Phys. Chem.*, 1971, **75**, 458.
22 T. Yamase and R. Watanabe, *J. Chem. Soc., Dalton Trans.*, 1986, 1669.
23 T. Yamase, *J. Chem. Soc., Dalton Trans.*, 1991, 3055.
24 D. M. Bartels, R. G. Lawler and A. D. Trifanac, *J. Chem. Phys.*, 1985, **83**, 2686.
25 M. D. E. Forbes, *J. Phys. Chem.*, 1992, **96**, 7836.
26 Y. Sakaguchi, H. Hayashi, H. Murai, Y. J. I'Haya and K. Mochida, *Chem. Phys. Lett.*, 1985, **120**, 401; Y. Sakaguchi, H. Hayashi, H. Murai and Y. J. I'Haya, *J. Phys. Chem.*, 1990, **94**, 291.

Received 31*st March* 1994; *Paper* 4/01977F